RSC Advances

PAPER

View Article Online
View Journal | View Issue



Cite this: *RSC Adv.*, 2023, **13**, 12654

# A novel non-enzymatic electrochemical uric acid sensing method based on nanohydroxyapatite from eggshell biowaste immobilized on a zinc oxide nanoparticle modified activated carbon electrode (Hap-Esb/ZnONPs/ACE)

Retno Wulandari, *[ab] Ardi Ardiansyah,[a] Henry Setiyanto [c] and Vienna Saraswaty *[a]

Received 23rd February 2023
Accepted 11th April 2023

DOI: 10.1039/d3ra01214j

rsc.li/rsc-advances

Hydroxyapatite-derived eggshell biowaste (Hap-Esb) has been fabricated and developed for the electrochemical detection of uric acid (UA). The physicochemical characteristics of the Hap-Esb and modified electrodes were evaluated using a scanning electron microscope and X-ray Diffraction analysis. Utilized as UA sensors, the electrochemical behavior of modified electrodes (Hap-Esb/ZnONPs/ACE) was assessed using cyclic voltammetry (CV). The superior peak current response observed for the oxidation of UA at Hap-Esb/ZnONPs/ACE, which was 13 times higher than that of the Hap-Esb/activated carbon electrode (Hap-Esb/ACE) is attributed to the simple immobilization of Hap-Esb on zinc oxide nanoparticle-modified ACE. The UA sensor exhibited a linear range at 0.01 to 1 μM, low detection limit (0.0086 μM), and excellent stability, which surpass the existing Hap-based electrodes reported in the literature. The facile UA sensor subsequently realized is also advantaged by its simplicity, repeatability, reproducibility, and low cost, applicable for real sample analysis (human urine sample).



## Introduction

In the current field of disease diagnosis and treatment, there is a necessity to create a device that can identify, trace, and quantify the metabolites of several important biochemical processes in the human body for a fast, straight forward, and accurate diagnosis of a variety of disorders. Uric acid (UA) and its derivatives are required for biological activity in the human body. UA is a natural antioxidant and by product of purine metabolism.[1,2] Excess UA concentration is associated with a number of diseases including gout, cardiovascular,[3] hyperuricemia,[4] and type II diabetes.[5] Meanwhile, a lower amount of UA than its typical range may reflect an earlier stage of Parkinson's, Alzheimer's, or multiple sclerosis disease.[6,7] Therefore, a device that can monitor UA has become important.

Several analysis methods, including high performance liquid chromatography,[8,9] chemiluminescence analysis,[10] spectrophotometry,[11] and electrochemical analysis, have been used for UA analysis.[12,13] Among them, electrochemical analysis has received more attention because of its fast, reliable, and accurate results.[14–18] To date, most electrochemical UA sensing is enzymatic. This is because the UA molecules can react with a specific enzyme, uricase, resulting in good selectivity in the detection of UA.[19,20] However, enzymatic sensing has several limitations, for example, the enzyme must be placed at a specific temperature (typically at 3–4 °C), have a short lifetime, and must be packed properly.[21,22]

Studies have proposed applying hydroxyapatite (Hap) as a non-enzymatic sensor for electrochemical detection of UA.[23–25] Hap is a calcium phosphate compound with the chemical formula $Ca_{10}(PO_4)_6(OH)_2$. It can be synthesized by various techniques, including deposition, hydrolysis, hydrothermal synthesis, and/or extraction from natural resources, for example, eggshells, seashells, shrimp shells, bovine bones, and fish bones.[26–28] Because of the high demand for eggs in food production, there is an abundance of eggshell biowaste (Esb). An eggshell is structurally composed of three layers: the cuticle, the spongy layer, and the lamellar layer.[29,30] The spongeous and lamellar layers resemble a matrix of protein fibers tied to the calcium carbonate (calcite) crystal at a ratio of 1 : 50. The calcite content of an eggshell is approximately ~94% wt, making it a good candidate for valorizing into Hap and using as UA sensing for electrochemical detection.[23,31,32]

[a]*Research Center for Applied Microbiology, National Research and Innovation Agency Republic of Indonesia, Bandung, Indonesia. E-mail: vien001@brin.go.id*

[b]*Chemical Engineering Department, Faculty of Engineering, Universitas Bhayangkara Jakarta Raya, Jl. Harsono RM No. 67, Jakarta, Indonesia. E-mail: Retno.wulandari@ubharajaya.ac.id*

[c]*Analytical Chemistry Research Group, Institut Teknologi Bandung, Bandung, Indonesia. E-mail: setiyanto@itb.ac.id*

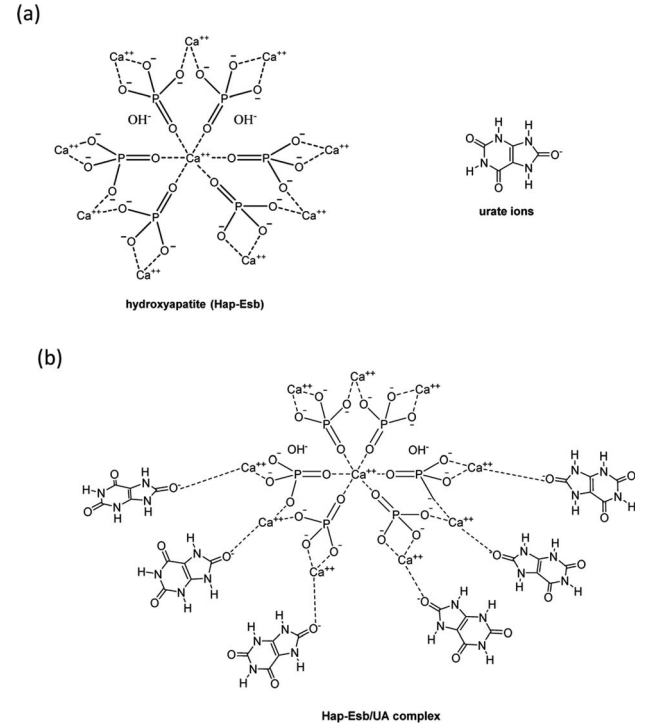


Fig. 1 (a) Chemical structures of hydroxyapatite (Hap-Esb) and urate ions. (b) And proposed Hap-Esb/UA complexes.

The chemical structure of Hap and urate ions is presented in Fig. 1(a). As shown, the Hap has positive charges from Ca ions, while urate ions are negatively charged. Therefore, it is assumed that urate ions can be adsorbed onto the positively charged molecule of Hap, forming the Hap-UA complex (see Fig. 1(b)). However, as can be seen, in the Hap chemical structure, the negatively charged ions that are from the hydroxyl group (OH–) are also present. The (OH–) ions appear to play a significant role in electrochemistry thereby increasing the current response (reduction).[32–37] Therefore, Hap could be used for the detection of UA with further modification of the electrode surface by applying a semiconductor material to improve the current response.

Among various metal oxides, zinc oxide (ZnO) is a very promising semiconductor material.[38] This is because ZnO has high electrocatalytic activity that facilitates better electron transport.[16,39–44] The high isoelectric point of ZnO doubtless enables the improvement absorption of analytes, result in a greater current response.[45–49] More importantly, ZnO is an environmentally friendly, cheap, highly stable material (both physically and chemically), biocompatible, and non toxic material.[47,50,51] For the aforementioned reasons, we are interested in applying ZnO to modify our sensing.

In general, Hap can easily combine with the carbon family. Activated carbon, carbon nanotubes, and graphene are known for providing improved performance as supercapacitor electrodes.[52–54] Activated carbon (AC) is frequently used as an electrode in the production of supercapacitors because AC has numerous advantages including inexpensive, easy to find, has a high porosity and highly scalable.[55–57] As a result, in this present work, we further modify the Hap-Esb with ZnO nanoparticles and AC to create a non-enzymatic UA sensing system. The structure and surface morphology of the as synthesized Hap was characterized by scanning electron microscopy (SEM) and X-ray diffraction (XRD). While the performance of our proposed sensor in UA detection was evaluated by cyclic voltammetry (CV). In order to provide a feasibility study, we also observed the CV profiles of the urine sample as the real sample analysis.

## Experimental section

### Materials and instruments

Eggshell biowastes (Esb) were collected from the food waste located in Bandung City, Indonesia. Activated carbon, ZnONPs used were from the previous work. $KH_2PO_4$ (≥99.995%), and $K_2HPO_4$ (≥99.99%) are from Merck (Germany) with a pro analytical grade. Ultrapure water was prepared by a Module E-pure D4642-33 instrument (Barnstead) with a resistivity ≥18 MΩ.

The surface morphology of Hap-Esb, as well as electrode surface modification were observed using scanning electron microscopy (SEM; JEOL JSM IT300, Japan). The formation of Hap-Esb and the size of its crystallites were assessed using X-ray diffraction (XRD) patterns obtained with the D-8 Advance (Bruker) instrument. The Autolab PGSTAT101 Metrohm was used to record the electrochemical measurement.

### CaO extraction and synthesis of Hap-Esb

In this investigation, the Esb were collected from a local market located (Bandung City, West Java, Indonesia) and rinsed repeatedly with tap water to remove impurities and dried under the sun. After drying, the clean Esb was crushed into coarse powder and then sieved with a 100-mesh size. The Esb powder was then transferred into a crucible to be calcinated at 1000 °C for 5 h in a furnace. Later, for the synthesis of Hap-Esb, about 21.23 g of CaO from Esb was dispersed in 500 mL of ultrapure water. Following that, 0.6 M $H_3PO_4$ was added to the solution at a flow rate of 6 mL $min^{-1}$ until the ratio reached 1 : 1. The suspension was heated for 1 h, at 60 °C. The pH of the solution was adjusted to pH 10 by adding 25% v/v ammonia. Then the suspension was sonicated for 1 h (40 kHz) and kept at room temperature (RT) for overnight. Subsequently, the filtrate was separated by centrifugation (3000 rpm, 15 min). The precipitates were then collected and dried overnight in an oven at 105 °C. The dried precipitates were transferred to a crucible and calcined at 1000 °C for 5 hours. The as-synthesized Hap-Esb powders were then collected and characterized by SEM and XRD.

### Preparation of bare and modified electrodes

Bare activated carbon electrode (ACE) was prepared by grinding 0.5 g of AC powder in a mortar with 100 μL paraffin oil for 30 minutes until a homogeneous paste was formed. Then the paste was packed into a capillary tube. A cooper wire was inserted into the capillary tube for electrical contact. The Hap-Esb/ZnO/ACE

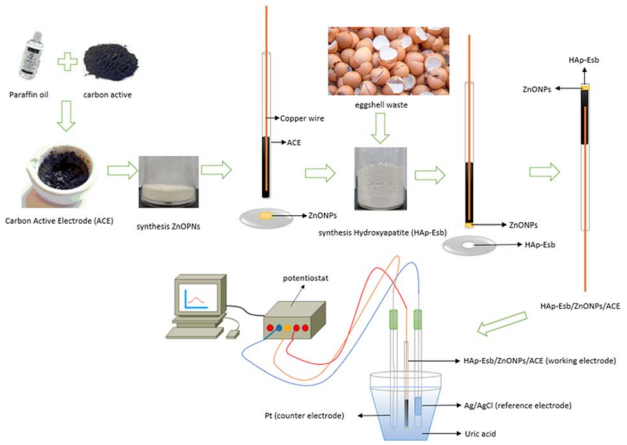


Fig. 2 Schematic preparation of the Hap-Esb/ZnONPs/ACE.

and Hap-Esb/ACE were prepared by a simple immobilization of the as-synthesized ZnONPs[58] and Hap on the surface of ACE. The schematic preparation of Hap-Esb/ZnO NPs/ACE is presented in Fig. 2.

### Electrochemical measurements

A computerized potentiostat instrument (PGSTAT101 Metrohm, AutoLab) was linked to a computer equipped with software, NOVA 1.11 with a three-electrode cell (30 mL capacity) was employed for electrochemical measurement. A Pt-wire electrode (CE) (6.0301.100 Metrohm, AutoLab) and an Ag/AgCl reference electrode (RE) (6.0729.100 Metrohm, AutoLab) and the working electrode (WE) Hap-Esb/ZnONPs/ACE were used.

The cyclic voltammetry technique was used to study the electrochemical behavior as well as to evaluated the performance of the developed electrode using UA standard solutions and a healthy human urine sample for real sample analysis. The potentials window of −1.5 V to 1.8 V and a scan rate of 100 mV $s^{-1}$ was employed. The UA standard solutions were prepared in 0.1 M phosphate buffer solution (PBS) pH 8, with various concentrations (0.01–1 μM). The sensor performance was also evaluated in the presence of interfering compounds that are ascorbic acid, glucose and tyrosine to confirm the selectivity in UA detection.

## Results and discussion

### Characterization of Hap-Esb

CaO was extracted from Esb by calcining the Esb for 5 hours at 1000 °C. High temperatures will decompose and eliminate the spongeous and lamellar matrix that are not thermally stable and are linked with the calcite from the eggshell.[59,60] And the calcite from the Esb will be transformed into CaO in accordance with the reaction eqn (1).

$$CaCO_3 \rightarrow CO_2 + CaO \quad (1)$$

The Hap-Esb was synthesized by mixing the CaO from Esb with a 0.6 M $H_3PO_4$ solution, followed by calcination at 1000 °C for 5 h. The heating stage is very important for the formation of Hap-Esb. The use of higher temperature, the more Hap produced.[61] To confirm the formation of Hap from Esb (Hap-Esb), the XRD analysis was employed. The X-ray diffraction (XRD) pattern of the as-synthesized Hap-Esb was displayed in Fig. 3. The as-synthesized Hap-Esb clearly showed intense peaks at 2$\theta$ values of 10.84, 16.99, 21.85, 22.84, 25.84, 27.82, 28.91, 31.75, 32.16, 32.88, 34.03, 35.59, 38.53, 40.41, 41.96, 46.80, 49.44, 49.58, and 52.05 are assigned to (100), (101), (200), (111), (002), (102), (210), (211), (112), (300), (202), (301), (220), (310), (131), (113), (222), (213), and (322) planes respectively, matching with Hap JCPDS pattern of 9-432 (ref. 62) (see Fig. 3(a)). Next, the crystallite sizes of Hap-Esb were calculated using the Debye Scherer formula (see eqn (2)),

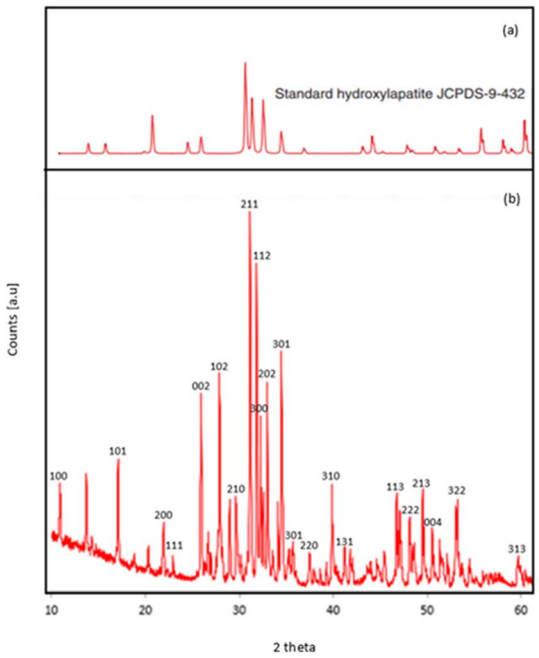


Fig. 3 XRD pattern of (a) Hap (JCPDS card no. 9-432); (b) products Hap from eggshell obtained by precipitation method.

$$D = \frac{0.9\lambda}{\beta \cos \theta} \quad (2)$$

where '$D$' is denotes for the crystallite size, $\lambda$ is the X-ray wavelength (1.54178 Å), '$\beta$' is the full width half maximum (FWHM) of the peak, and '2$\theta$' is the Bragg angle.[63] The calculation of crystallite sizes from Hap-Esb was tabulated in Table 1. As presented, the calculated crystallite size of Hap-Esb was found in the range of ∼48 to ∼107 nm. And the average of Hap-Esb crystallite sizes was ∼78 nm. The XRD analysis suggests that the as-synthesized Hap-Esb are nanoparticles.

Fig. 4(a) shows an SEM image of as-synthesised Hap-Esb. As shown at 5000× magnification, the as-synthesized Hap-Esb were found in a mixture of coral shapes constructed with hexagonal rods and square tile-like shapes.[64,65] Additionally, the Hap-Esb particles were found to agglomerate. The surface morphology of the modified ACE with ZnONPs is presented in Fig. 4(b). The ZnO NPs were indicated with white dots. From

Table 1 Calculation of crystallite size of Hap from eggshell

| 2 theta position | Crystallite size (nm) |
|---|---|
| 10.84 | 48.89 |
| 16.99 | 65.65 |
| 21.85 | 66.12 |
| 22.84 | 99.31 |
| 25.84 | 66.61 |
| 27.82 | 100.29 |
| 28.91 | 67.05 |
| 31.75 | 67.50 |
| 32.16 | 101.31 |
| 32.88 | 101.50 |
| 34.03 | 101.80 |
| 35.59 | 51.12 |
| 38.53 | 103.12 |
| 40.41 | 103.73 |
| 41.96 | 52.13 |
| 46.80 | 70.74 |
| 49.44 | 107.17 |
| 49.58 | 53.61 |
| 52.05 | 72.75 |
| Average | 78.97 |

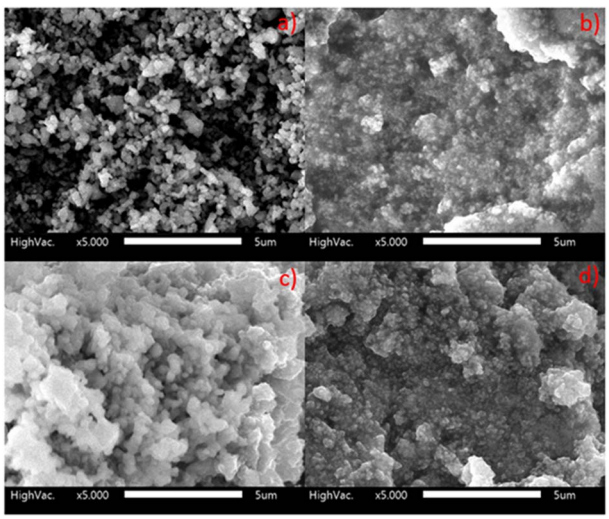


Fig. 4 SEM images of (a) Hap synthesis from eggshell (Hap-Esb); (b) ZnONPs/ACE; (c) Hap-Esb/ZnONPs/ACE before used; (d) Hap-Esb/ZnONPs/ACE after used at 5000× magnification.

Fig. 4(b), it can be seen that the ZnO NPs are successfully attached to the surface of ACE and well dispersed. The surface morphology of Hap-Esb/ZnONPs/ACE is depicted in Fig. 4(c). As shown, white and cloudy particles are submicron in size and connected one to another, indicating an agglomeration of Hap-Esb particles.[33,66–68] There are several factors that can cause agglomeration are (1) shear forces between particles, (2) initial density, (3) moisture, (4) sintering temperature, and (5) particle size.[69–72] In this work, the synthesis procedure of Hap-Esb and the preparation of the developed electrode include grinding, wetting, and drying processes, possibly causing the agglomeration. The influence of particle size in agglomeration is emphasized by the calculation of Hap-Esb crystallite size by the Debye–Scherer equation, which suggests that the Hap-Esb are nanoparticles. Undoubtedly, they tend to agglomerate.[63,71] Fig. 4(d) shows the surface morphology of Hap-Esb/ZnONPs/ACE after measurement. As shown, the Hap-Esb particles are detached from the ZnONPs-ACE surface, suggesting an instability issue after measurement.

### Cyclic voltammetry (CV) behavior of the modified electrode toward UA response

CV technique was applied to study the electrochemical behavior of the modified electrode toward 0.1 μM UA response in 0.1 M PBS solution (pH 8, potential range of −1.5 to 1.8 V, and a scan rate of 100 mV $s^{-1}$). The cyclic voltammograms (CVs) for 0.1 μM UA at the bare ACE, Hap-Esb/ACE, ZnONPs/Hap-Esb/ACE, and Hap-Esb/ZnONPs/ACE are presented in Fig. 5(a). There were a good response in the peak at −0.53 V corresponding to UA electro-oxidation. The data showed that the greatest peak oxidation current response was observed at the Hap-Esb/ZnONPs/ACE (111.48 μA) surface in comparison with the bare ACE (30.6 μA), Hap-Esb/ACE (8.10 μA), and ZnONPs/Hap-Esb/ACE (24.02 μA) (see Fig. 5(b)), indicating the improved sensitivity of the developed electrode towards UA detection. It is very imperative to note that the layer arrangement on surface modification is significantly affects the currents response.[73] When the ZnONPs layer was brought forward on the outermost surface of the developed sensor (ZnONPs/Hap-Esb/ACE), the ZnONPs blocked the Hap-Esb pore, reducing the current response. In reverse, when the ZnONPs were sent backward between Hap-Esb and ACE (Hap-Esb/ZnONPs/ACE), the current

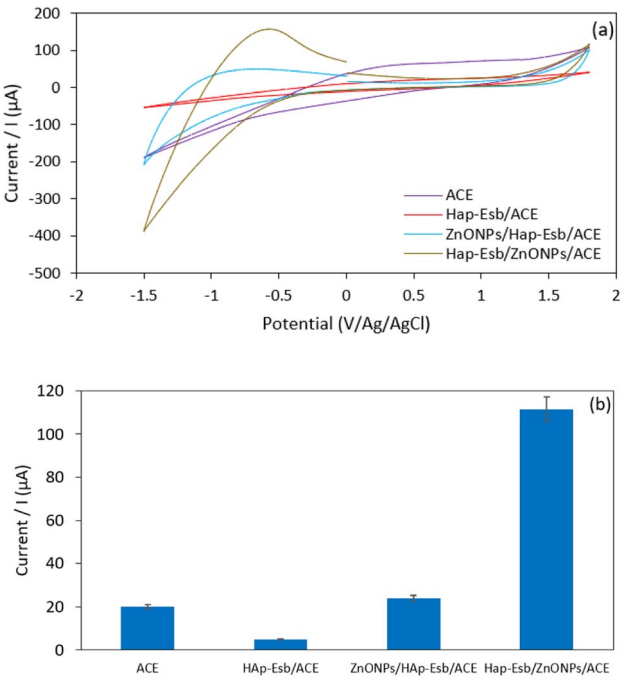


Fig. 5 (a). The CV voltammogram and (b) histogram of peak current response of the bare, Hap-Esb, ZnONPs/Hap-Esb/ACE and Hap-Esb/ZnONPs/ACE.

response was significantly higher than the bare ACE as well as the ZnONPs/Hap-Esb/ACE. Factors that affect the electrochemical response are (1) analyte diffusion, (2) catalysts, and (3) electron transfer.[74] By placing the Hap at the outermost surface, this improves the diffusion of UA and promotes the complexation of urate ions with $Ca^{2+}$ from the Esb-Hap.[37,52] And the immobilization of ZnO NPs in the middle layer improves electron transfer, resulting in the highest current response.

## Optimization of HAp-Esb/ZnONPs/ACE

**The influence of pH.** In electro-analytical evaluation, the pH of the solution significantly influences the current response since the protons are involved in the reaction.[75] Over a pH range of 3 to 9, the effect of pH on the peak current response of UA at the Hap-Esb/ZnONPs/ACE in 0.1 M PBS was observed. Fig. 6 depicts CVs recorded in the presence of 0.1 μM UA at a scan rate of 100 mV $s^{-1}$. The results show that the peak current response of UA increases gradually from pH 3 to 8, which can be attributed to the fact that Hap slowly dissolves in acidic solutions. It is also known that the $Ca^{2+}$ ions of Hap-Esb form a complex with urate ions (see Fig. 1(b)).[76,77] As a result, when Hap dissolves slowly in an acidic environment, it loses its ability to bond the urate ions, resulting in a lower current response. The maximum oxidation UA current was obtained at pH 8. Therefore, PBS at pH 8 was used as the electrolyte in subsequent experiments.

**Calibration plot and limit of detection.** A calibration plot was constructed to assist the quantitative calculation of UA in real samples using the most proficient electrodes, Hap-Esb/ZnONPs/ACE. Fig. 7(a), presents the CV voltammograms recorded using HAp/ZnONPs/ACE at various concentrations of UA, from 0.01–1 μM (Fig. 7(b)), in a 0.1 M phosphate buffer at pH 8.0. It can be concluded from Fig. 7(c), that the current response ($I_p$) increases linearly with the concentration of UA in that range, with the linear regression equation of $I_p$ (μA) = 1160.5$x$ + 78.238 and $R^2$ = 0.9946.

We noticed that at concentrations of 0.01 to 1.0 μM, the peak current response tends to be flat (Fig. 7(b)); this is probably due to the saturation of the recognition site on the electrode surface.[37,78] The limit of detection (LOD) was determined as "3da/$b$", where 'da' is the standard error of the intercept, and '$b$' is the slope of the calibration curve, while the LOQ was calculated by "10da/$b$". The limit of detection (LOD) and limit of quantification (LOQ) were estimated to be 0.0086 μM and 0.028 μM, respectively. The linear current response and the LOD value obtained in this study are compared with the literature and presented in Table 2. As tabulated in Table 2, the proposed Hap-Esb based sensor is superior to those available in the literature, as suggested by the lowest LOD value. Therefore, our work creates a proof that Hap-Esb has the potential to be used as a component of a sensor.

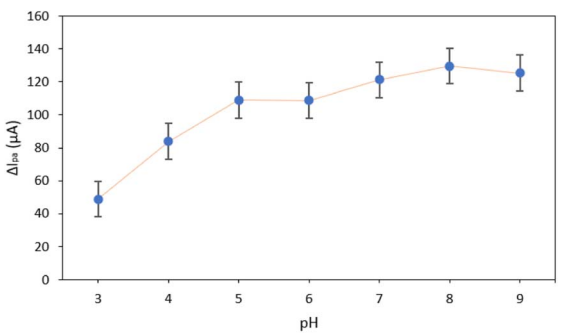


Fig. 6 The anodic peak current response of 0.1 μM UA at the Hap-Esb/ZnONPs/ACE in PBS at pH ranging from 3 to 9.

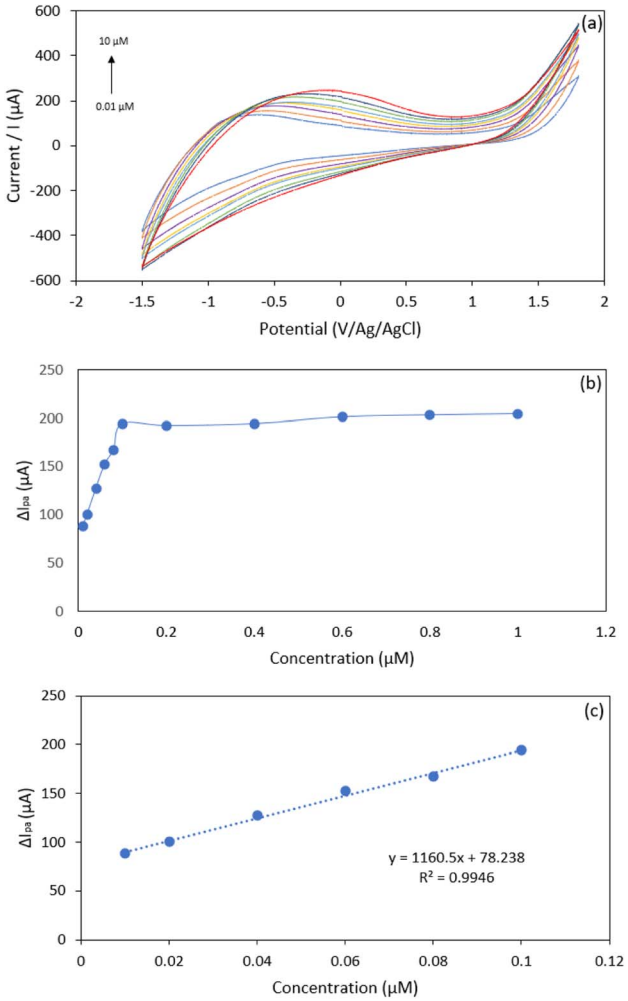


Fig. 7 (a) CV voltammogram of UA at 0.01–10 μM; (b) plot of UA concentration (0.01–1 μM) *vs.* anodic peak current; (c) plot of UA concentration (0.01–0.1 μM) *vs.* anodic peak current.

## Reproducibility, repeatability, and stability of the developed electrode

Reproducibility, repeatability, and stability all played important roles in sensor performance. In this investigation, four equally prepared electrodes were tested to detect UA by using 0.1 μM UA solution by CV for reproducibility evaluation. The relative standard deviation (RSD) of the peak current response of UA was found to be 0.24%. Next, we tested the developed sensor for 20 repetitive measurements to confirm the instability issue

Table 2 Comparison of the proposed uric acid sensor with literature reports

| Electrode | pH | Linear range | Detection limit | Ref. |
|---|---|---|---|---|
| Hap-Esb/ZnONPs/ACE | 8.0 | 0.01 to 10 μM | 0.0086 μM | This work |
| HA/GCE | 7.0 | 0.1 to 30.0 μM | 0.142 μM | 79 |
| Graphene-modified carbon fiber | 7.0 | 0.194 to 49.68 μM | 0.132 μM | 22 |
| Pretreated-CPE | 7.0 | 5 to 53.0 μM | 5.0 μM | 80 |
| Carbon ionic liquid | 6.8 | 2 to 220 μM | 1.0 μM | 81 |
| Ce-HA/GCE | 7.0 | 0.5 to 200 μM | 0.39 μM | 25 |
| Poly(DPA)/$SiO_2$@$Fe_3O_4$-CPE | 7.0 | 1.2 to 8.2 μM | 0.4 μM | 18 |
| Graphite-like pyrolytic carbon film | 7.0 | 0.1 to 9.8 μM | 0.03 μM | 82 |
| RGO-ZnO/GCE | 6.0 | 1.0 to 70.0 μM | 0.33 μM | 83 |
| Poly(bromocresol purple)/GCE | 6.5 | 0.5 to 120 μM | 0.20 μM | 17 |
| Nitrogen doped graphene | 6.0 | 0.1 to 20.0 μM | 0.045 μM | 84 |
| $LaPO_4$/CPE | 7.0 | 2.7 to 24.0 μM | 0.09 μM | 85 |
| Graphene/size-selected Pt nanocomposites/GCE | 7.0 | 0.05 to 11 μM | 0.05 μM | 86 |
| N-rGO | 7.0 | 1.0 to 30.0 μM | 0.20 μM | 15 |
| PCN/MWCN | 4.8 | 0.2 to 4.0 μM | 0.139 μM | 87 |
| n-HA/CPE | 7.0 | 0.068 to 50 μM | 0.05 μM | 23 |

suggested by the SEM image. The CV and histogram of repetitive testing were presented in Fig. 8. Before the repeating test, the developed sensor was washed with ultrapure water using the CV for 3 cycles to remove the analyte. The CV curve of the first measurement and the 15th measurement were compared. As shown in Fig. 8(a), the recorded voltammograms at $n = 1$ and $n = 15$ were almost similar. And the calculation of RSD value for 15 repetitive measurement result in 1.5% RSD, indicating excellent repeatability performance. We recorded that at the 20$^{th}$ measurement, the peak current decreased (see Fig. 8(b)). This was probably due to the detachment of Hap from the electrode surface. For the aforementioned reason we suggest the prepared electrode is stable for 15 repetitive measurement.

Next, we also observed the stability of the developed electrode by comparing the UA peak current response measured using freshly prepared and stored electrodes. For this analysis, the electrode was stored for 3 months in a desiccator. The results of comparative measurement can be seen in Fig. 8(c). As presented, the UA peak current responses of freshly prepared ($t = 0$) and stored ($t = 3$ months) are similar, as suggested by the oxidation peak current values of 206.8 μA and 217.3 μA for $t = 3$ months and $t = 0$, respectively. Those data show that the developed sensor can be stored for 3 months.

Interference study. Possible interferences for the detection of UA at Hap-Esb/ZnONPs/ACE were evaluated by spiking UA with various interfering species. In this work, the selectivity performance of Hap-Esb/ZnONps/ACE towards UA was evaluated in the presence of glucose, ascorbic acid, and tyrosine. Those interferings are coexisting molecules present in the human biological fluids. The interfering species were first tested individually to detect any possibility of overlapping signals. As shown in Fig. 9, the CV of UA, AA, glucose, tyrosine, UA + AA, UA + glucose, UA + tyrosine, and UA + AA + glucose + tyrosine depicted the peak current response at potentials of −0.32 V, −0.49 V, −0.46 V, −0.53 V, −0.55 V, −0.44 V, −0.83 V and −0.72 V, respectively (see Fig. 9(a)). The peaks of the current responses of UA were found to be 217.3 μA, 180.9 μA, 173.8 μA, 216 μA, 193.4 μA, 204.6 μA, 208.6 μA and 248.7 μA when

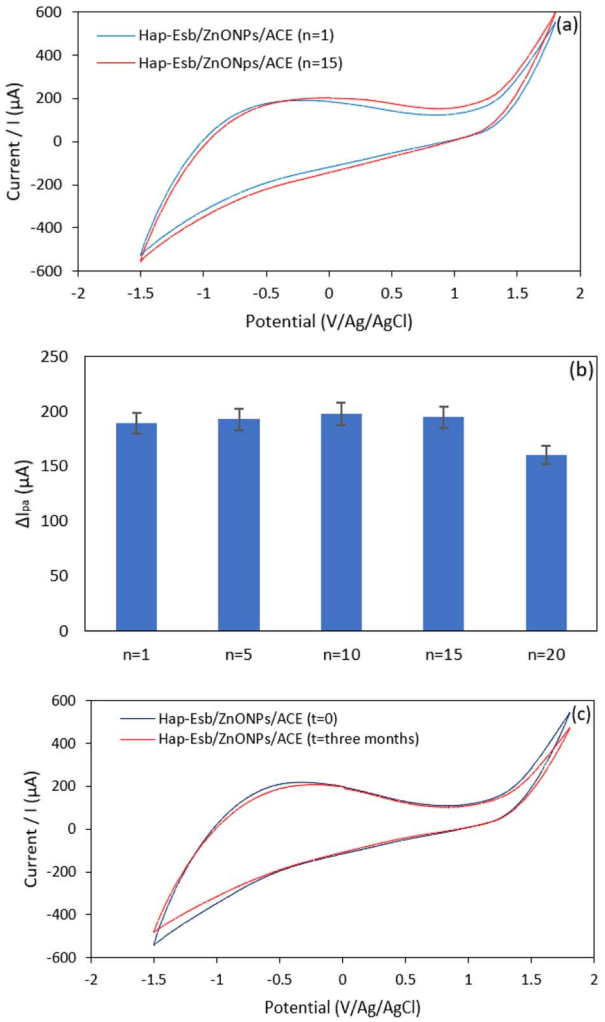


Fig. 8 (a) CV voltammograms of 0.1 μM UA at $n = 1$ and $n = 15$ and (b) the histogram of oxidation peak current of 0.1 μM UA at various repetitive measurement at Hap-Esb/ZnONPs/ACE; and (c) CV of UA measured using Hap-Esb/ZnONPs/ACE at different electrode stored for 0 and 3 months.

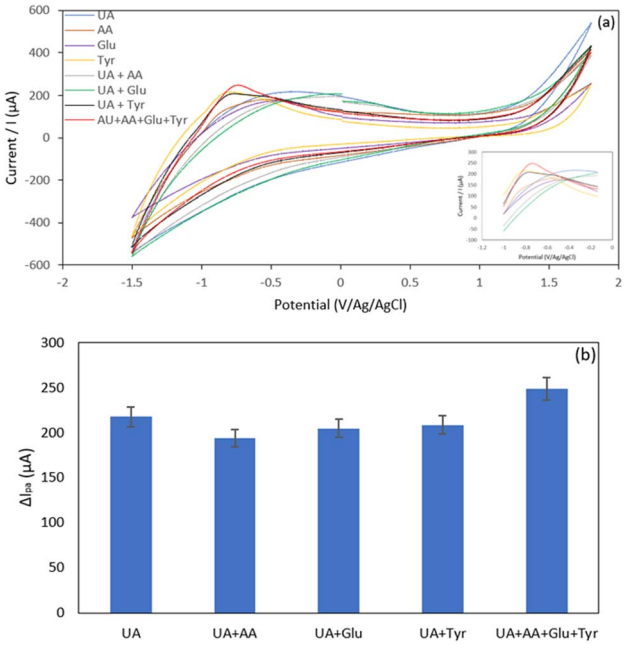


Fig. 9 (a) Voltammogram of 0.2 μM interferent molecules on Hap-Esb/ZnONPs/ACE; (b) histogram of oxidation peak current of 0.2 μM interferent molecules on Hap-Esb/ZnONPs/ACE.

measured under unspiking and spiking conditions (see Fig. 9(b)). Notably, the presence of glucose and AA decreased the peak current response. In the pH optimization analysis, the pH value obviously influences the peak response of UA at Hap-Esb/ZnO/ACE (see Fig. 6). The presence of AA appears to increase the acidity and decreasing current response.[87,88] Whereas the decrease of UA peak current response in the presence of glucose might be due to the competition between glucose and UA to fill the cavity of Hap-Esb.[16,23,25,87,89] We also noticed that the presence of tyrosine increased the peak current response.[25] Given that the difference of peak current responses are less than 10% (between 1–9.15%), our proposed sensor shows a remarkably selectivity.

Finally, the developed sensor is applied to test UA in a real sample. In this work, we apply human urine samples. The urine samples were diluted 100 times with 0.1 M PBS pH 8. The dilution process aims to reduce as well as to eliminate the effect of metabolites present in the urine. As presented in Fig. 10, the CV voltammogram of the urine sample is similar with the UA standard solutions. The peak potential of the UA response from the urine sample was found at −0.13 V, with a peak current response of 291 μA. From the calculation results, the concentration of UA in urine is equivalent to 10.08 mg $dL^{-1}$ with an RSD value of 4.4%. This results is within the range of UA concentration for healthy human urine. The results obtained were compared using the high-performance liquid chromatography (HPLC) method, with a result of 10.12 mg $dL^{-1}$. The Hap-Esb/ZnONPs/ACE electrode was able to detect UA in urine samples (10.08 mg $dL^{-1}$) with results that were not significantly different when using the HPLC method (10.12 mg $dL^{-1}$). So we suggest that the proposed sensor promising for monitoring UA in real samples.

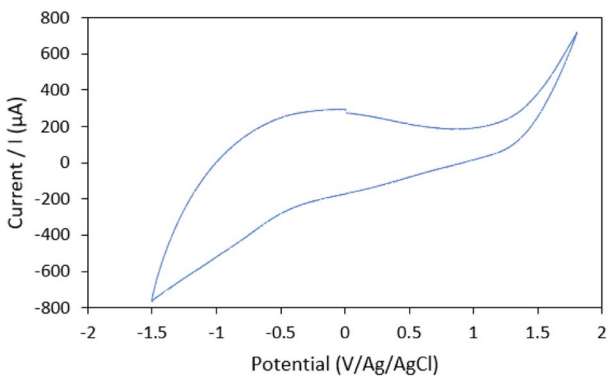


Fig. 10 CV voltammogram of UA from human urine for real sample analysis at Hap/ZnONPs/ACE.

## Conclusions

In summary, an electrochemical sensing-based Hap-Esb/ZnONPs/ACE is developed for detection of UA. A simple immobilization of Hap-Esb on ZnONPs/ACE is used to modify the electrode. Electrochemical studies show that the developed electrode exhibits excellent response for UA detection in PBS at pH 8 in the presence of interferings. The linear dynamic range of UA is 0.01–1 μM with a LOD value of 0.0086 μM at the developed electrode. It is observed that the repeatability performance of the developed electrode is verified, as suggested by a similar response after 15 repetitive CV tests. Most interestingly, the current response of UA is improved up to 13 times higher by combining the Hap-Esb with ZnONPs, suggesting a better electrocatalytic activity. Considering similar CV response of UA in real sample evaluation, the proposed Hap-Esb/ZnONPs/ACE has a promising application for monitoring UA.

## Ethical statement

The authors state that for investigations involving human subjects were in compliance with relevant laws or guidelines and informed consent was obtained from all human subjects.

## Conflicts of interest

There are no conflicts to declare.

## Acknowledgements

The authors thank Research Center for Applied Microbiology and Advanced Characterization Laboratories BASICS at KST Samaun Samadikun, National Research and Innovation Agency Republic of Indonesia through e-Layanan Sains and Bhayangkara Jakarta Raya University. This research is partly supported by Project of Riset and Inovasi untuk Indonesia Maju (RIIM) with contract No. 82/II.7/HK/2022 under VS and PostDoctoral Program of Direktorat Manajemen Talenta BRIN with Contract No. 64/II/HK/2022 under RW.

## References

1 L. L. Jiang, X. Gong, M. Y. Ji, C. C. Wang, J. H. Wang and M. H. Li, *Foods*, 2020, **9**(8), 1–24.
2 Y. Wu, P. Deng, Y. Tian, J. Feng, J. Xiao, J. Li, J. Liu, G. Li and Q. He, *J. Nanobiotechnol.*, 2020, **18**, 112.
3 M. Kuwabara, *Pulse*, 2015, **3**, 242–252.
4 W. L. Nyhan, *Tzu Chi Med. J.*, 2007, **19**, 105–108.
5 A. Dehghan, M. Van Hoek, E. J. G. Sijbrands, A. Hofman and J. C. M. Witteman, *Diabetes Care*, 2008, **31**, 361–362.
6 I. I. Hidayat, L. Hamijoyo and M. A. Moeliono, *Indones. J. Rheumatol.*, 2013, **04**, 14–19.
7 X. L. Jin Jun Luo, *Brain Disord. Ther.*, 2013, **02**, 109–111.
8 K. Inoue, T. Namiki, Y. Iwasaki, Y. Yoshimura and H. Nakazawa, *J. Chromatogr. B: Anal. Technol. Biomed. Life Sci.*, 2003, **785**, 57–63.
9 X. Dai, X. Fang, C. Zhang, R. Xu and B. Xu, *J. Chromatogr. B: Anal. Technol. Biomed. Life Sci.*, 2007, **857**, 287–295.
10 C. Yang and Z. Zhang, *Talanta*, 2010, **81**, 477–481.
11 D. R. Norton, M. A. Plunkett, F. A. Richards and M. A. Plunkett, *Anal. Chem.*, 1954, **26**, 454–457.
12 F. Mazzara, B. Patella, G. Aiello, A. O'Riordan, C. Torino, A. Vilasi and R. Inguanta, *Electrochim. Acta*, 2021, **388**, 138652.
13 J. Lv, C. Li, S. Feng, S.-M. Chen, Y. Ding, C. Chen, Q. Hao, T.-H. Yang and W. Lei, *Ionics*, 2019, **25**, 4437–4445.
14 D. R. Norton, M. A. Plunkett and F. A. Richards, *Anal. Chem.*, 1954, **26**, 454–457.
15 H. Zhang and S. Liu, *J. Alloys Compd.*, 2020, 155873.
16 D. Lakshmi, M. J. Whitcombe, F. Davis, S. Sharma and B. Prasad, *Electroanalysis*, 2011, 305–320.
17 Y. Wang and L. Tong, *Sens. Actuators, B*, 2010, **150**, 43–49.
18 Y. Veera Manohara Reddy, B. Sravani, S. Agarwal, V. K. Gupta and G. Madhavi, *J. Electroanal. Chem.*, 2018, **820**, 168–175.
19 B. Govindan, R. Madhu, S.-M. Chen, V. Veeramani, A. Balamurugan, D. Mangalaraj, C. Viswanathan and P. Nagamony, *J. Mater. Chem. B*, 2015, **3**(7), 1360–1370.
20 R. Jirakunakorn, S. Khumngern, J. Choosang, P. Thavarungkul, P. Kanatharana and A. Numnuam, *Microchem. J.*, 2020, **154**, 104624.
21 H. Zhu, L. Li, W. Zhou, Z. Shao and X. Chen, *J. Mater. Chem. B*, 2016, **4**, 7333–7349.
22 J. Du, R. Yue, Z. Yao, F. Jiang, Y. Du, P. Yang and C. Wang, *Colloids Surf., A*, 2013, **419**, 94–99.
23 E. Iyyappan, S. J. Samuel Justin, P. Wilson and A. Palaniappan, *ACS Appl. Nano Mater.*, 2020, **3**, 7761–7773.
24 P. Kanchana and C. Sekar, *Mater. Sci. Eng., C*, 2014, **42**, 601–607.
25 P. Kanchana, M. Navaneethan and C. Sekar, *Mater. Sci. Eng., B*, 2017, **226**, 132–140.
26 P. S. L. Pandharipande, *Int. J. Adv. Inf. Sci. Technol.*, 2016, **52**, 36–47.
27 E. M. Rivera, M. Araiza, W. Brostow, V. M. Castaño, J. R. Díaz-Estrada, R. Hernández and J. R. Rodríguez, *Mater. Lett.*, 1999, **41**, 128–134.
28 K. Lin and J. Chang, *Structure and Properties of Hydroxyapatite for Biomedical Applications*, Elsevier Ltd., 2015, vol. 4214.
29 A. S. M. Bashir and Y. Manusamy, *J. Eng. Res. Technol.*, 2016, **2**, 2015.
30 M. T. Hincke, Y. Nys, J. Gautron, K. Mann, A. B. Rodriguez-Navarro and M. D. McKee, *Front. Biosci.*, 2012, **17**, 1266–1280.
31 C. X. Wang, M. Wang and X. Zhou, *Biomaterials*, 2003, **24**, 3069–3077.
32 Z. Zyman, J. Weng, X. Liu, X. Li and X. Zhang, *Biomaterials*, 1994, **15**, 151–155.
33 G. Bharath, R. Madhu, S.-M. Chen, V. Veeramani, A. Balamurugan, D. Mangalaraj, C. Viswanathan and N. Ponpandian, *J. Mater. Chem. B*, 2015, **3**, 1360–1370.
34 J. J. K. Ngouoko, K. Y. Tajeu, R. C. T. Temgoua, G. Doungmo, I. Doench, A. K. Tamo, T. Kamgaing, A. Osorio-Madrazo and I. K. Tonle, *Materials*, 2022, **15**(12), 1–17.
35 A. Khalil, A. Almajid and M. Soliman, *Mater. Sci. Appl.*, 2011, **02**, 105–110.
36 G. Bharath, A. Naldoni, K. H. Ramsait, A. Abdel-Wahab, R. Madhu, E. Alsharaeh and N. Ponpandian, *J. Mater. Chem. A*, 2016, **4**, 6385–6394.
37 T. Tite, A. C. Popa, L. M. Balescu, I. M. Bogdan, I. Pasuk, J. M. F. Ferreira and G. E. Stan, *Materials*, 2018, **11**, 1–62.
38 R. Verma, S. Pathak, A. K. Srivastava, S. Prawer and S. Tomljenovic-Hanic, *J. Alloys Compd.*, 2021, **876**, 160175.
39 T. Sen, S. Mishra, S. Sonawane and N. Shimpi, *Polym. Eng. Sci.*, 2018, **58**(8), 1438–1445.
40 V. S. Bhati, M. Hojamberdiev and M. Kumar, *Energy Rep.*, 2020, **6**, 46–62.
41 K. Shi and K.-K. Shiu, *Electroanalysis*, 2001, **13**, 1319–1325.
42 B. Uslu, *Open Chem. Biomed. Methods J.*, 2011, **3**, 56–73.
43 M. Ghaedi, S. Y. S. Jaberi, S. Hajati, M. Montazerozohori, M. Zarr, A. Asfaram, L. K. Kumawat and V. K. Gupta, *Electroanalysis*, 2015, **27**, 1516–1522.
44 M. Ganjali, *Int. J. Electrochem. Sci.*, 2017, **12**, 3231–3240.
45 T. Kokab, A. Shah, M. A. Khan, M. Arshad, J. Nisar, M. N. Ashiq and M. A. Zia, *ACS Appl. Nano Mater.*, 2021, **4**, 4699–4712.
46 D. Wingett, P. Louka, C. B. Anders, J. Zhang and A. Punnoose, *Nanotechnol., Sci. Appl.*, 2016, **9**, 29–45.
47 M. L. M. Napi, S. M. Sultan, R. Ismail, K. W. How and M. K. Ahmad, *Materials*, 2019, **12**(18), 1–34.
48 Z. Wang, H. Li, F. Tang, J. Ma and X. Zhou, *Nanoscale Res. Lett.*, 2018, **13**, 202.
49 M. S. Rahmanpour and M. A. Khalilzadeh, *Sensors*, 2016, **8**, 922–930.
50 Y. Zhao, Z. Wang, R. Yuan, Y. Lin, J. Yan, J. Zhang, Z. Lu, D. Luo, J. Pietrasik, M. R. Bockstaller and K. Matyjaszewski, *Polymer*, 2018, **137**, 370–377.
51 S. Chaudhary, A. Umar, K. K. Bhasin and S. Baskoutas, *Materials*, 2018, **11**, 1–38.
52 P. R. Dev, C. P. Anand, D. S. Michael and P. Wilson, *Mater. Adv.*, 2022, 7773–7809.
53 T. Mutuk and M. Gürbüz, *J. Compos. Mater.*, 2021, **55**, 3087–3097.

54 M. Magni, D. Sironi, M. Ferri, S. Trasatti, S. Campisi, A. Gervasini, M. Papacchini and P. Cristiani, *ChemElectroChem*, 2023, **202201017**, 1–11.
55 S. Joseph, D. M. Kempaiah, M. R. Benzigar, H. Ilbeygi, G. Singh, S. N. Talapaneni, D. H. Park and A. Vinu, *Microporous Mesoporous Mater.*, 2019, **280**, 337–346.
56 I. Švancara and K. Kalcher, *Adv. Electrochem. Sci. Eng.*, 2016, **16**, 379–423.
57 E. Pérez-Mayoral, I. Matos, M. Bernardo and I. M. Fonseca, *Catalysts*, 2019, **9**(2), 1–35.
58 H. Setiyanto, P. Faradilla, R. Manurung and V. Saraswaty, *RSC Adv.*, 2022, **12**, 743–752.
59 D. Cree and P. Pliya, *J. Build. Eng.*, 2019, **26**, 100852.
60 F. Murakami, P. Rodrigues, C. Campos and M. Silva, *Cienc. Tecnol. Aliment.*, 2007, **27**(3), 658–662.
61 M. Marraha, J. C. Heughebaert and M. Heughebaert, *Phosphorus, Sulfur Silicon Relat. Elem.*, 1993, **79**, 281–291.
62 M. Tagaya, T. Ikoma, N. Hanagata, D. Chakarov, B. Kasemo and J. Tanaka, *Sci. Technol. Adv. Mater.*, 2010, **11**, 45002.
63 S. Fatimah, R. Ragadhita, D. F. Al Husaeni and A. B. D. Nandiyanto, *ASEAN J. Sci. Eng.*, 2021, **2**, 65–76.
64 F. Hilbrig and R. Freitag, in *Biopharmaceutical Production Technology, Volume 1 & Volume 2*, 2012, vol. 1, pp. 283–331.
65 A. Afshar, M. Ghorbani, N. Ehsani, M. R. Saeri and C. C. Sorrell, *Mater. Des.*, 2003, **24**, 197–202.
66 J. J. K. Ngouoko, K. Y. Tajeu, R. C. T. Temgoua, G. Doungmo, I. Doench, A. K. Tamo, T. Kamgaing, A. Osorio-Madrazo and I. K. Tonle, *Materials*, 2022, **15**(12), 1–17.
67 S. Das Lala, P. Deb, E. Barua, A. B. Deoghare and S. Chatterjee, *Mater. Today: Proc.*, 2019, **15**, 323–327.
68 T. V. Gopal, T. M. Reddy, P. Shaikshavali and G. Venkataprasad, *Surf. Interfaces*, 2021, **24**, 101145.
69 M. Manoj, R. Subbiah, D. Mangalaraj, N. Ponpandian, C. Viswanathan and K. Park, *Nanobiomedicine*, 2015, **2**, 1–11.
70 M. Tourbin, F. Brouillet, B. Galey, N. Rouquet, P. Gras, N. Abi Chebel, D. Grossin and C. Frances, *Powder Technol.*, 2020, **360**, 977–988.
71 F. Wu, D. D. W. Lin, J. H. Chang, C. Fischbach, L. A. Estroff and D. Gourdon, *Cryst. Growth Des.*, 2015, **15**, 2452–2460.
72 C. Wang and S. H. Chen, *Acta Mech. Sin. Xuebao*, 2012, **28**, 711–719.
73 L. Khalafi, *Cyclic Voltammetry*, 2017.
74 N. Thakur, D. Mandal and T. C. Nagaiah, *J. Mater. Chem. B*, 2021, **9**, 8399–8405.
75 T. Kawasaki, *J. Chromatogr. A*, 1991, **544**, 147–184.
76 G. Viscusi, G. Barra and G. Gorrasi, *Cellulose*, 2020, **27**, 8653–8665.
77 G. Bharath, A. J. Kumar, K. Karthick, D. Mangalaraj and C. Viswanathan, *RSC Adv.*, 2014, **4**, 37446–37457.
78 Q. Yan, N. Zhi, L. Yang, G. Xu, Q. Feng, Q. Zhang and S. Sun, *Sci. Rep.*, 2020, 1–10.
79 P. Kanchana and C. Sekar, *Mater. Sci. Eng., C*, 2014, **42C**, 601–607.
80 X. Cai, K. Kalcher, C. Neuhold and B. Ogorevc, *Talanta*, 1994, **41**, 407–413.
81 A. Safavi, N. Maleki, O. Moradlou and F. Tajabadi, *Anal. Biochem.*, 2006, **359**, 224–229.
82 M. Hadi and A. Rouhollahi, *Anal. Chim. Acta*, 2012, **721**, 55–60.
83 X. Zhang, Y. Zhang and L. Ma, *Sens. Actuators, B*, 2016, **227**, 488–496.
84 Z. Sheng, X. Zheng, J. Xu, W. Bao, F. Wang and X. Xia, *Biosens. Bioelectron.*, 2012, **34**, 125–131.
85 Y. Zhou, H. Zhang, H. Xie, B. Chen, L. Zhang, X. Zheng and P. Jia, *Electrochim. Acta*, 2012, **75**, 360–365.
86 C. Sun, H. Lee, J. Yang and C. Wu, *Biosens. Bioelectron.*, 2011, **26**, 3450–3455.
87 J. Lv, C. Li, S. Feng, S. M. Chen, Y. Ding, C. Chen, Q. Hao, T. H. Yang and W. Lei, *Ionics*, 2019, **25**, 4437–4445.
88 N. Tukimin, J. Abdullah and Y. Sulaiman, *Sensors*, 2017, **17**(7), 1–12.
89 M. Khasanah, H. Darmokoesoemo, N. Widayanti, Y. Kadmi, H. Elmsellem and H. S. Kusuma, *Results Phys.*, 2017, **7**, 1833–1844.